A Deep Neural Network based MU-MIMO Beamforming Training Protocol for IEEE 802.11ay

Mun-Suk Kim, Tanguy Ropitault, SuKyoung Lee, Jun-Hyeok Choi, and Nada Golmie

Abstract—IEEE 802.11ay supports a multi-user multiple-input-multiple-output (MU-MIMO) beamforming training (BFT); hence, an access point (AP) can perform data transmissions simultaneously with multiple stations (STAs). During MU-MIMO BFT, the AP sends a significant number of action frames to the STAs to determine appropriate directional antenna patterns. However, if transmit sectors (TSs) used in the transmission of action frames are selected inefficiently, the AP could perform redundant transmissions; this could eventually lead to the poor performance of the MU-MIMO BFT in terms of signaling and latency overhead. To select the appropriate TSs, the AP is required to accurately estimate the link qualities measured at the STAs when certain TSs are used simultaneously to transmit an action frame. Therefore, in this study, we propose a deep neural network (DNN)-based scheme that performs efficient MU-MIMO BFT. It achieves this by accurately estimating link qualities measured at the STAs when an action frame is transmitted through multiple TSs. Moreover, it performs this function without collecting any additional channel information that is not specified in the standard. For performance evaluation, we conducted extensive simulations with realistic mmWave channel and antenna array models in four indoor and outdoor propagation scenarios. The simulation results demonstrate that our scheme transmits fewer action frames and achieves a lower BFT time than existing schemes.

Index Terms—Beamforming training, deep neural networks, IEEE 802.11ay, MU-MIMO.

I. INTRODUCTION

WITH constantly growing data traffic driven by high-rate applications such as high-definition video streaming and virtual reality gaming, millimeter wave (mmWave) communication is crucial to meeting the throughput and latency requirements of such applications [1]. While mmWave technologies have abundant spectrum resources, their transmissions must be directional in order to handle high attenuation characteristics [2]; recently, the 802.11ay has been standardized to address this challenge and enables wireless local area network (WLAN) devices to achieve transmission rates of up to 100 Gbps in the 60 GHz band [3].

To realize transmission rates in the order of tens of Gbps, 802.11ay supports a downlink multi-user multiple-input-multiple-output (DL MU-MIMO) transmission. This means that an access point (AP) can send multiple data streams simultaneously to multiple stations (STAs). The MU-MIMO transmission must be directional and, to this end, the AP performs MU-MIMO beamforming training (BFT) with the STAs, which has already been defined as an multi-user (MU) group [3], [4]. Specifically, the AP splits the MU group into one or more subgroups of STAs and determines each transmit antenna weight vector (AWV) to be used when performing DL MU-MIMO transmission with each subgroup; the AP then informs the STAs in the MU group about respective receive AWVs to be used when the STAs in each subgroup receive DL MU-MIMO transmission. During the procedure of the MU-MIMO BFT specified in the IEEE 802.11ay standard, the AP is required to send a significant number of action frames to the STAs; the action frames include parameters for the setup, training, feedback, and selection subphases of the BFT phase. The standard states that the minimum number of action frames should be transmitted in the MU-MIMO BFT; however, the standard does not specify how the AP selects transmit sectors (TSs), or precomputed AWVs, to transmit an action frame. All vendors need to address the problem of selecting the TSs used in the transmission of action frames to improve the performance of MU-MIMO BFT in terms of signaling and latency overhead [5]–[7].

Studies [4] and [5] provided a summary of the MU-MIMO BFT protocol specified in the 802.11ay standard, focusing on the formats of action frames and signaling procedures. The authors of [8]–[10] developed novel algorithms to determine beam patterns for simultaneous transmission of multiple spatial streams; In particular, their proposed algorithms were designed to reduce inter-stream interference. Other studies [11] and [12] formulated beam alignment problems to determine the optimal beam parameters that achieved minimum latency. Fixed wireless access has been investigated in [13] and [14], which described key elements incorporated into IEEE 802.11ay, including beamforming and link maintenance. For IEEE 802.11ay dense environments, [15] and [16] designed advanced protocols for adjustable BFT with the aim of shortening the BFT time. Furthermore, a recent study [2] described efficient BFT algorithms formulated as a first-order Markov process that supports multiple beam pairs, exploiting the

M. Kim and J.-H Choi are with the Department of Computer Sciences and Engineering, Sejong University, Seoul, 05006, South Korea, email: msk@sejong.ac.kr, chlwns1023@gmail.com.

T. Ropitault, and N. Golmie are with the National Institute of Standards and Technology, Gaithersburg, MD 20899 USA, email: {tanguy.ropitault, nada.golmie}@nist.gov.

S. Lee is with the Department of Computer Science, Yonsei University, Seoul 03722, South Korea, e-mail: sklee@yonsei.ac.kr.

S. Lee is the corresponding author.

spatial-temporal consistency of the mmWave channel.

While the aforementioned studies investigated the details of the directional transmission protocols in the mmWave channel, they did not address the problem of selecting the TSs used in the transmission of action frames during the MU-MIMO BFT, which is referred to as the *transmit antenna configuration*. Our prior studies [6] and [7] introduced transmit antenna configuration schemes for the MU-MIMO BFT protocol specified in the standard. The IEEE 802.11ay standard defines transmitter blocks through which the bit stream of an action frame is transmitted using multiple antenna arrays applying a spatial expansion with cyclic shift diversity [3]; the cyclic shift diversity enables the AP to achieve transmit antenna gain resulting from the use of multiple antenna arrays at a time. Moreover, a mmWave channel between the AP and each STA is characterized by the line-of-sight component as well as a few reflected and diffracted components. Hence, when multiple beams are simultaneously transmitted through multiple antenna arrays, the multipath components of each single beam may cause inter-symbol interference (ISI).

The scheme of [6] uses multiple antenna arrays simultaneously to transmit an action frame; to this end, it selects the TSs of respective transmit antenna arrays based on the signal to noise ratio (SNR) measured with every single TS. However, the scheme of [6] cannot consider the effect of ISI and the cyclic shift diversity; hence, it is limited by the accuracy of estimation of SNR to be measured at each STA when multiple TSs are used simultaneously. This causes the AP to be unable to identify STAs within reach of the transmission of an action frame, leading to redundant transmissions thereby increasing the signaling and latency overhead during the MU-MIMO BFT. In contrast, the scheme of [7] estimates accurate SNRs based on the channel information that each STA calculates by leveraging the auto-correlation property of a Golay complementary pair. However, the scheme of [7] includes an additional overhead of collecting the channel information because this procedure is not specified in the standard.

To overcome the limitations of our previous studies, we propose a deep neural network (DNN) based transmit antenna configuration (DTAC) scheme for MU-MIMO BFT. Using a DNN, our DTAC scheme estimates the qualities of the ISI links to be measured when an action frame is transmitted through multiple TSs simultaneously. In contrast to the previous study [7], our scheme does not collect any information on the channel between the AP and each STA. Instead, our DTAC scheme collects, as inputs of the DNN, link qualities measured with every single TS of the AP which is the existing BFT operations specified in the standard. Thus, our proposed scheme can effectively identify STAs within reach of the transmission of the action frame, while maintaining lower signaling and latency overhead during the BFT compared to the existing schemes.

Finally, we conducted extensive simulations to accurately evaluate our DTAC scheme and compare its performance with that of existing schemes [6], [7]. Specifically, the mmWave channel was implemented with a quasi-deterministic (Q-D) channel model based on NIST and TGay measurement campaigns. As described in previous studies [19]–[20], extensive channel measurement campaigns were conducted in specific indoor and outdoor environments with mmWave channel sounders. This was done because the mmWave channel is sparse and can be represented by clustered multipath components. Through the measurement campaigns, the properties of the clustered multipath components were primarily investigated in the delay-angle space.

The remainder of this paper is structured as follows. In Section II, we review related work on the MU-MIMO BFT and mmWave channel models. Section III describes the proposed DTAC scheme. In Section IV, we present the simulation results and discuss the performance of our DTAC scheme and compare it to existing schemes. Finally, Section V concludes the paper.

II. BACKGROUND AND CONTRIBUTIONS

In this section, we briefly present the procedure of MU-MIMO BFT specified in the standard and then describe how the existing methodologies improve the performance of the BFT and discuss the limitations of the existing ones. We also present prior studies that use deep learning approaches to improve the performance of the BFT. It is important to model the mmWave channel for the precise evaluation of the proposed and existing schemes; we introduce three broad categories of mmWave channel models and explain how the channel models were used in the existing studies. Finally, the major contributions of this study are summarized.

A. MU-MIMO BFT Schemes and Their Limitation

The 802.11ay standard defines the MU-MIMO BFT procedure [3], and the procedure has been summarized in a number of studies including [4]–[7]. The MU-MIMO BFT procedure commences with the single-input-single-output (SISO) phase, followed by the MIMO phase, as shown in Fig. 1.

The SISO phase comprises two consecutive subphases: transmit sector sweep and SISO feedback. In the transmit sector sweep subphase, the AP transmits short sector sweep (SSW) frames through different TSs of each of its transmit antenna arrays, and each STA measures SNRs corresponding to the SSW frames. The AP subsequently collects SNRs during the SISO feedback subphase.

There are four subphases in the MIMO phase: BF setup, BF training, BF feedback, and BF selection. During the MIMO phase, the AP transmits a significant number of action frames to the STAs. The action frames transmitted in the BF setup subpahse contain parameters, such as TSs that will be trained; the ones transmitted in the BF training subpahse include TRN fields to test candidate transmit AWVs [21]. In the BF feedback subphase, the AP collects the feedback for the test performed during the BF training subpahse; finally, the action frames transmitted in the BF selection subphase contain information regarding the receive AWVs to be used for DL MU-MIMO transmission.

However, the 802.11ay standard does not specify the method to select the appropriate TSs used in the transmissions of these action frames [3]. To select appropriate TSs, the AP needs to
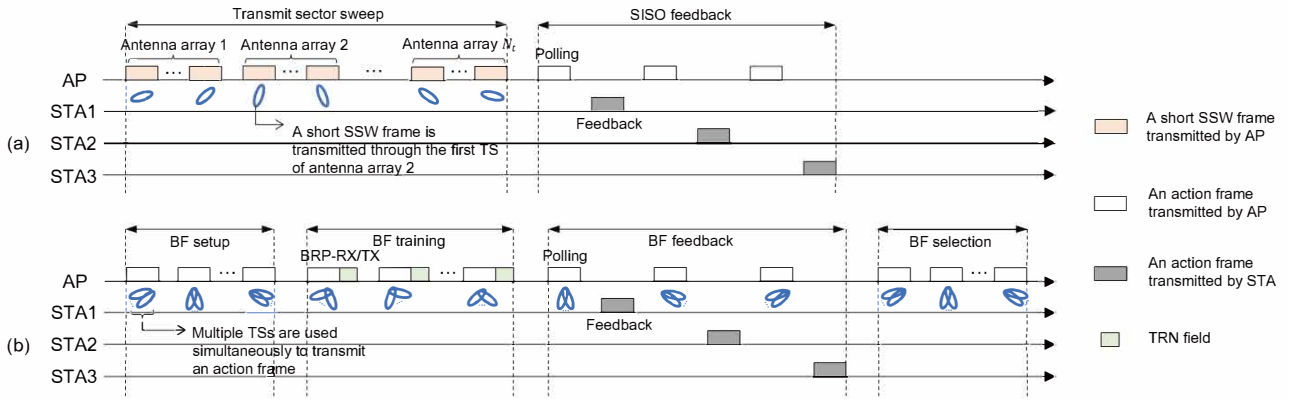
Fig. 1. The procedure of the MU-MIMO BFT specified in the IEEE 802.11ay standard: (a) SISO and (2) MIMO phases.

accurately identify STAs within the reach of an action frame transmitted through the TSs simultaneously. For example, in the case of the BF setup or selection subphase, the AP is required to continue transmitting copies of an action frame until all STAs in the MU group have received the action frame; however, if the AP is incapable of identifying STAs within the reach of each transmission, this causes the AP to perform redundant transmissions.

The schemes in [6] and [7] select multiple TSs to be used simultaneously to transmit an action frame. In [6], the SNRs corresponding to TSs, which were included in the SISO feedback, were considered to identify the reach of the action frame. Specifically, the LSB scheme in [6] selects the TSs with the largest SNRs to transmit an action frame, whereas the LNS scheme in [6] selects the TSs through which the transmission can reach the largest number of STAs. However, in the LSB and LNS schemes, the AP is incapable of ensuring that an action frame transmitted throughput multiple TSs reaches STAs. This is because these schemes only utilize the SNR corresponding to each single TS; hence, the LSB and LNS schemes cannot consider the effect of the ISI channel incurred when multiple TSs are used simultaneously.

The study [7] developed the ILQE scheme that selects the TSs similarly as the LNS scheme; however, in contrast to the LNS scheme, the ILQE scheme accurately estimates the quality of the links between the AP and the STAs by considering the transmit diversity of the ISI channel. To this end, the ILQE scheme includes an additional overhead of collecting the channel information which is not specified in the standard.

B. DNN Schemes for Beamforming Training

Deep learning approaches have been used in some studies [22]–[24] to reduce the beam training overhead especially in terms of computational complexity. The study [22] proposed a deep learning-based beam selection scheme with low overhead by virtue of the super-resolution technology; this super-resolution-inspired deep learning constructs the beam qualities and received powers of narrow beams based on the wide-beam measurements. In [23], a learning-based adjustable beam training scheme was proposed to intelligently and flexibly select beam training candidates according to user mobility

and propagation scenarios. The scheme in [23] can achieve real-time performance by constructing parallel multiple deep learning networks to determine training candidates dynamically. The study [24] proposed a deep learning-based beam management and interference coordination scheme for the concurrent use of directional transmission in dense mmWave networks; this scheme transforms a conventional complex beam management and interference coordination algorithm into a simple deep neural network-based approximation.

C. Millimeter Wave Channel Modeling

Determining the TSs used in the transmission of action frames plays a crucial role in making MU-MIMO BFT efficient [6], [7]. To evaluate the performance of the transmit antenna configuration, the modeling of the mmWave channel is required to accurately calculate SNRs measured at STAs for the transmission of action frames. There are three broad categories of mmWave channel models: analytical, stochastic, and quasi-deterministic [25].

The performance of the LSB and LNS schemes was evaluated using the analytical channel model. Analytical studies for the mmWave channel have typically employed simplified equations to calculate the SNRs [6], [26], [27], and [28]. Moreover, these studies considered transmit and receive beamforming gains and path loss that were modeled by equations or random distributions. However, analytical channel models limit the representation accuracy of multipath components with realistic antenna arrays [25]. In stochastic spatial channel models, multipath components are generated from a set of random distributions with parameters determined by experimental measurements on the mmWave channel [29]. Stochastic spatial channel models have also been widely used. One example is the 3GPP channel model in [30], although these models can be applied in a common rural or urban scenario, they are inaccurate in specific indoor scenarios, such as a lecture room [25].

Finally, in the Q-D channel model, direct and reflected multipath components were characterized with high accuracy in the given environments; therefore, the Q-D channel model was adopted by the IEEE 802.11ay task group [19]. The ILQE scheme was evaluated using the Q-D channel model [7], and this evaluation was more accurate than that of the LSB and

LNS schemes. In this study, our proposed scheme is evaluated with more realistic antenna arrays and accurate measurement campaigns, compared to [7]. Furthermore, the evaluation was conducted in four indoor and outdoor scenarios with their own propagation characteristics.

D. Contributions

We can summarize the major contributions of this study as follows:

First, we present a deep learning model to accurately estimate the SNRs measured at STAs when an action frame is transmitted during MU-MIMO BFT. The proposed DTAC scheme refrains from collecting any additional channel information during the SISO phase, in contrast to the ILQE scheme and provides an estimation as accurate as the ILQE scheme. Thus, our proposed scheme transmits fewer redundant action frames and allow more STAs to engage in the BFT by capturing the benefit of the transmit diversity gain; in addition, it reduces the possibility of transmission failure, in comparison to the LSB and LNS schemes.

Second, we develop a heuristic method to reduce the number of times SNRs is estimated from our proposed deep learning model; hence, we can significantly reduce the computation overhead for MU-MIMO BFT.

Third, we conduct extensive simulations with an antenna model more realistic than that in the existing studies in [6] and [7], as mentioned in Section II-C; in particular, we consider the orientation and rotation of antenna arrays and their respective positions. In addition, to ensure precise evaluation, we model correlated channels based on the distance between the two antenna arrays.

Fourth, for implementing the Q-D channel, we consider *diffuse* rays, in addition to the deterministic and specular rays used in the study [7], where diffuse rays are generated owing to the scattering of specular rays from rough surfaces. In Section IV, we have described how the diffuse rays cluster around the specular rays and are modeled stochastically with TGay or NIST measurement; similar to that in [17], [25], and [31], we performed ray-tracing simulations to obtain the properties of clustered specular and diffuse rays in the four indoor and outdoor scenarios of lecture room, L-shaped room, hotel lobby, and street canyon, which have different propagation characteristics [32]. We then conducted link abstraction to calculate the bit error rate in control mode communication specified in the IEEE 802.11ay standard, referring to studies [33] and [34]. Finally, we performed system-level simulations with network simulator (ns-3), which supports the procedure of MU-MIMO BFT specified in the standard by extending the findings of works [35] and [36].

III. DNN Based Transmit Antenna Configuration for MU-MIMO BFT

This section presents our proposed DTAC scheme to solve the problem of selecting an appropriate precomputed AWVs for the MU-MIMO BFT, in which each selected set of TSs is used to transmit an action frame.

We first introduce the overall operation of our DTAC scheme. We then describe how our DTAC scheme utilizes DNN to estimate the SNRs of the candidate sets of TSs. Following this, we explain the heuristic algorithm that determines the transmit antenna configuration for each subphase of MU-MIMO BFT while reducing the computational complexity. Finally, we present an example scenario for easy comprehension.

A. Overall Operation of DTAC Scheme

We assume a sub-connected architecture where each radio frequency (RF) chain is associated with its own single-antenna array [7]. As specified in [3] and [37], a spatial expansion with cyclic shift diversity is applied to transmit the action frame; hence, the bit stream of an action frame is mapped to all RF chains. Eventually, the bit stream of each RF chain is transmitted via the antenna array connected to the RF chain.

Fig. 2 describes the overall operations of our proposed DTAC scheme. (1) It utilizes the SNRs corresponding to TSs, which have been fed back from each STA in the SISO phase; these SNRs are exploited to estimate SNRs corresponding to candidate sets of TSs to be used to transmit action frames for the MIMO phase. The computational complexity of our DTAC scheme depends on the number of times the SNRs corresponding to candidate sets of TSs have to be estimated. (2) In our heuristic algorithm, a lookup table is used to reduce the number of times the SNRs are estimated from a pretrained DNN; our scheme can easily initialize the lookup table using the SISO feedback. (3) Using the lookup table, our scheme selects sets of TSs to be used for the transmission of action frames in the MIMO phase. (4) To check whether the selected sets of TSs are appropriate, our scheme employs the pretrained DNN; if inappropriate, our scheme updates the relevant SNRs in the lookup table and then re-selects sets of TSs.

B. Deep Neural Network based SNR Estimation

The SISO feedback contains a list of TSs detected when each STA receives the SSW frames and SNRs corresponding to the detected TSs, as shown in Fig. 2(1). Our proposed DTAC scheme utilizes multiple TSs simultaneously to transmit an action frame. Accordingly, our DTAC scheme estimates the SNR to be measured at each STA for the multiple TSs. This estimation is based on the SNRs measured with every single TS, which is known from the SISO feedback.

We use a multilayer perceptron neural network to estimate the SNR of the multiple concurrent beams; each layer, except the last one, is fully connected to the next, and there are no connections within a layer. The first layer contains the input, and it can be presented as a tuple (R_{fb}^u, R_c^u), where R_{fb}^u is the set of SNRs measured at STA u when the action frame is transmitted through every single TS, and R_c^u is a set of SNRs that represents SNRs corresponding to TSs in a candidate set of multiple TSs c. Let r_α^u be the SNR corresponding to TS α. Then, $r_\alpha^u \in R_{fb}^u$ is the SNR corresponding to TS α in the SISO feedback of STA u, provided that TS α is included in the SISO feedback; otherwise, r_α^u is zero. For TSs in the candidate set c, the set R_c^u includes the same SNRs as those in the set R_{fb}^u;
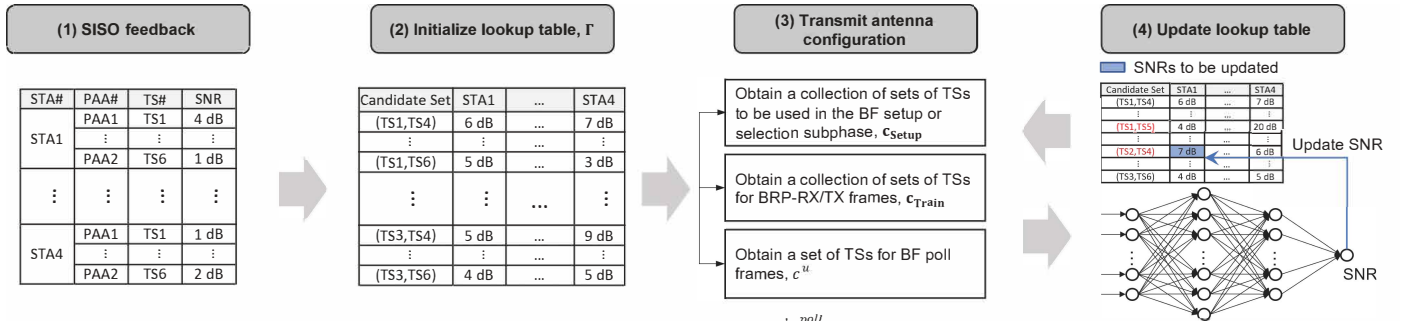
Fig. 2. Procedure of our DTAC scheme: (1) SISO feedback, (2) initialization of table Γ, (3) transmit antenna configuration, and (4) update of table Γ.

TABLE I
NOTATIONS FOR THE MODELING AND ANALYSIS OF MU-MIMO BFT.

| Notation	Description
N_t	Number of transmit antenna arrays
δ_{mu}	SNR threshold, i.e., the minimum SNR that guarantees reliable transmission
$\mathbf{u}_{\text{Tot}}$	Set of all STAs in the MU group
$\mathbf{c}_{\text{Tot}}$	Collection of all candidate sets of TSs
$\mathbf{c}_{\text{Setup}}$	Collection of sets of TSs to be used for the transmission of the BF setup or selection frames
$\mathbf{c}_{\text{Train}}$	Collection of sets of TSs to be used for the transmission of BRP-RX/TX frames in the BF training subphase
c_{poll}^u	Set of TSs to be used when transmitting a BF poll frame to STA u
R_{fb}^u	Set of SNRs measured at STA u when an action frame is transmitted through every single TS
R_c^u	Set of SNRs that represents SNRs corresponding to TSs in a candidate set $c \in \mathbf{c}_{\text{Tot}}$
r_α^u	SNR measured at STA u when an action frame is transmitted through TS α, i.e., $r_\alpha^u \in R_{fb}^u$
$\Gamma(u,c)$	SNR corresponding to STA u and candidate set c in the lookup table Γ
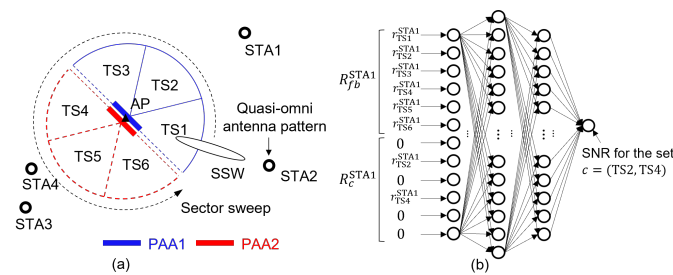
Fig. 3. (a) Example scenario for the transmit sector sweep of the SISO phase and (b) DNN when the candidate set c includes TSs 2 and 4.

however, for the other TSs, all the values of their SNRs are zero.

The final layer of the neural network contains the output; given the input (R_{fb}^u, R_c^u), the output conveys the SNR to be measured at STA u when the action frame is transmitted simultaneously through TSs in the set c. Intervening layers are referred to as hidden, and each hidden layer comprises a

random number of nodes.

C. Proposed Transmit Antenna Configuration

Our proposed DTAC scheme lists all candidate sets of TSs to be used to transmit action frames for the MIMO phase of MU-MIMO BFT. Let $\mathbf{c}_{\text{Tot}}$ denote a collection of all candidate sets of TSs; then, $\mathbf{c}_{\text{Tot}}$ comprises all combinations of TSs that are included in the SISO feedback received from at least one of the STAs in the MU group. Let $c \in \mathbf{c}_{\text{Tot}}$ be a candidate set of TSs; then, this set is given by $c = (\alpha_1, \cdots, \alpha_s, \cdots, \alpha_{N_t})$, where α_s is a TS associated with the sth antenna array and N_t is the number of transmit antenna arrays.

Subsequently, we create a lookup table that contains each SNR to be measured at each STA $u \in \mathbf{u}_{\text{Tot}}$ when all TSs in each candidate set $c \in \mathbf{c}_{\text{Tot}}$ are used simultaneously. Let Γ and $\Gamma(u,c)$ denote the lookup table and SNR to be measured at STA u for the candidate set c; then, $\Gamma(u,c)$ is estimated from the pretrained DNN, as described in Section III-B.

Once the lookup table Γ is given, our DTAC scheme determines sets of TSs, i.e., transmit antenna configurations, in a manner identical to that in [7]. These configurations will be used for each subphase of the MIMO phase. Hereinafter, $\mathbf{c}_{\text{Setup}}$ and $\mathbf{c}_{\text{Train}}$ denote the collection of sets of TSs to be used for the transmission of an action frame in the BF setup or selection subphase and for the transmissions of BRP-RX/TX frames, respectively; c_{poll}^u denotes a set of TSs to be used when transmitting a BF poll frame to STA u.

In particular, in the BF setup and selection subphases, the AP repeats the transmission of an action frame with a different set of TSs to ensure that all STAs in the MU group can receive the action frame. Thus, for each transmission, our DTAC scheme selects the corresponding set of TSs for which the transmission reaches the largest number of STAs that have not received the action frame in the MU group. Given the corresponding set $c \in \mathbf{c}_{\text{Tot}}$, our scheme considers STA u to be within the reach of the transmission if its SNR in the lookup table is greater than the SNR threshold, i.e., $\Gamma(u,c) > \delta_{mu}$. Then, let $\mathbf{u}_c$ denote the subgroup of STAs in the MU group that are within reach of an action frame transmitted through a candidate set c. To be concrete, for the transmit antenna configuration in the BF setup and selection subphases, our proposed scheme first selects a set of TSs c so that the

subgroup $\mathbf{u}_c$ includes the largest number of STAs; the set c can be obtained as follows:

$$c = \arg\max_{c' \in \mathbf{c}_{\text{Tot}}} |\mathbf{u}_{c'}|. \tag{1}$$

The selected set c is included in the collection $\mathbf{c}_{\text{Setup}}$ where $\mathbf{c}_{\text{Setup}}$ is initially set to ϕ. Our scheme then removes all STAs in the subgroup $\mathbf{u}_c$ from the set $\mathbf{u}_{\text{Tot}}$. If the set $\mathbf{u}_{\text{Tot}}$ becomes empty, our scheme finally obtains the collection $\mathbf{c}_{\text{Setup}}$; otherwise, it repeats the process by selecting a new set of TSs from (1) for the remaining STAs in the set $\mathbf{u}_{\text{Tot}}$.

In the BF training subphase of the MIMO phase, our proposed scheme determines the sets of TSs to be used for the transmissions of BRP-RX/TX frames to ensure that the AP performs BFT with all different subgroups of STAs in the MU group. Specifically, in the same manner as for the BF setup and selection subphases, our proposed scheme first selects a set of TSs c from (1); then, the selected set c is included in the collection $\mathbf{c}_{\text{Train}}$ where $\mathbf{c}_{\text{Train}}$ is initially set to ϕ. Subsequently, our scheme removes all sets c' from $\mathbf{c}_{\text{Tot}}$ if the subgroup associated with the selected set c includes the subgroup associated with the set c', i.e., if $\mathbf{u}_{c'} \subset \mathbf{u}_c$. If the collection $\mathbf{c}_{\text{Tot}}$ becomes empty, our scheme finally obtains the collection $\mathbf{c}_{\text{Train}}$; otherwise, it repeats the process by selecting a new set of TSs from (1) for the remaining sets in the collection $\mathbf{c}_{\text{Tot}}$.

In the BF feedback subphase, for each STA in the MU group, our DTAC scheme selects a set of TSs where the corresponding SNR is the highest in the lookup table. Then, the set of TSs to be used when transmitting a BF poll frame to STA u, can be obtained as follows:

$$c_{\text{poll}}^u = \arg\max_{c \in \mathbf{c}_{\text{Tot}}} \Gamma(u, c). \tag{2}$$

As mentioned earlier, the computational complexity of our proposed scheme is primarily determined by the number of estimates of SNRs corresponding to candidate sets of TSs. To reduce the complexity, our DTAC scheme employs a heuristic method, which significantly reduces the number of times SNRs is estimated from DNN. We assume that owing to the transmit diversity gain, the SNR of multiple concurrent beams is greater than that of the respective single beams but less than the sum of that of all single beams. Under this assumption, the heuristic algorithm selects the transmit antenna configuration for action frames transmitted in the MU-MIMO BFT by employing the SNRs of the respective single beams included in the SISO feedback. To check if the selected transmit antenna configuration is appropriate, our DTAC scheme estimates the corresponding SNRs, as described in Section III-B. The detailed operations are described in Algorithms 1 and 2.

D. Proposed DTAC Scheme in Example Scenario

We can consider the example scenario depicted in Figs. 2 and 3, where the AP has two phased antenna arrays (PAAs). Each PAA is associated with three TSs, and the MU group comprises four STAs, as shown in Fig. 3(a).

After the transmit sector sweep of the SISO phase is completed, the AP obtains SNRs corresponding to the respective
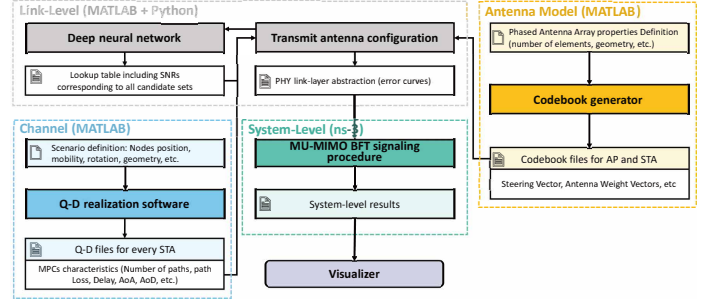

Fig. 4. Implementation of simulation programs with MATLAB, ns-3, and python [32].

single TSs from respective STAs. In Fig. 2(1), the first row of the table indicates that the SNR measured at STA1 is 4 dB when an action frame is transmitted through TS1 of PAA1.

Our DTAC scheme creates a lookup table and initializes it, as shown in Fig. 2(2). In the case of the candidate set $c = (\text{TS1}, \text{TS6})$, its SNR is set to the sum of the SNRs corresponding to TS1 and TS6 in Fig. 2(1); hence, for STA1, the SNR of the candidate set c is initialized to 5 dB, i.e., $4 \text{ dB} + 1 \text{ dB}$.

Considering the lookup table, our DTAC scheme determines the transmit antenna configurations $\mathbf{c}_{\text{Setup}}$, $\mathbf{c}_{\text{Train}}$, and c_{poll}^u, and subsequently checks whether the lookup table requires updating. Let us assume $\mathbf{c}_{\text{Setup}} = \{(\text{TS1}, \text{TS5}), (\text{TS2}, \text{TS4})\}$, $\delta_{mu} = 6$ dB, and $r_\delta = 0.5$ dB; $\mathbf{c}_{\text{Setup}} = \{(\text{TS1}, \text{TS5}), (\text{TS2}, \text{TS4})\}$ means that, for the BF setup or selection subphase, the AP transmits two action frames and, TS1 and TS5 (TS2 and TS4) are simultaneously used to transmit the first (second) action frame. In addition, we assume that the SNRs corresponding to TS2 and TS4 are 5 and 2 dB, respectively, for STA1 in the SISO feedback. Subsequently, as shown in Fig. 2(4), the SNR corresponding to candidate set $(\text{TS2}, \text{TS4})$ is 7 dB, i.e., $\Gamma(\text{STA1}, (\text{TS2}, \text{TS4})) = 7$ dB; however, this SNR should be updated because it is greater than the SNR threshold δ_{mu} and the respective SNRs of TS2 and TS4 are all less than δ_{mu} plus a predetermined margin value r_δ, as described in Algorithm 2. To update the value of $\Gamma(\text{STA1}, (\text{TS2}, \text{TS4}))$, our DTAC scheme utilizes DNN, as shown in Fig. 3(b). When the SISO feedback of STA1 is $R_{fb}^{\text{STA1}} = \{r_{\text{TS1}}^{\text{STA1}}, r_{\text{TS2}}^{\text{STA1}}, r_{\text{TS3}}^{\text{STA1}}, r_{\text{TS4}}^{\text{STA1}}, r_{\text{TS5}}^{\text{STA1}}, r_{\text{TS6}}^{\text{STA1}}\}$, the set of SNRs representing candidate set $(\text{TS2}, \text{TS4}) = c \in \mathbf{c}_{\text{Setup}}$ is $R_c^{\text{STA1}} = \{0, r_{\text{TS2}}^{\text{STA1}}, 0, r_{\text{TS4}}^{\text{STA1}}, 0, 0\}$. The tuple $(R_{fb}^{\text{STA1}}, R_c^{\text{STA1}})$ is used as the input for DNN, and $\Gamma(\text{STA1}, (\text{TS2}, \text{TS4}))$ is updated by the output SNR.

IV. PERFORMANCE EVALUATION

We evaluated our proposed DTAC scheme, and compared its results with those of the existing LSB, LNS, and ILQE schemes.

A. Simulation Setup

We utilized MATLAB, ns-3, and Python programs [32], as shown in Fig. 4, and the configuration and operation of the

---

Algorithm 1 Proposed DTAC algorithm for transmit antenna configuration

---

1: **for each** STA $u \in \mathbf{u}_{\text{Tot}}$ **and each** candidate set $c = \{\alpha_1, \cdots, \alpha_{N_t}\} \in \mathbf{c}_{\text{Tot}}$ **do**
2:     $\Gamma(u,c) \leftarrow \sum_{s=1}^{N_t} r_{\alpha_s}$;   // Initially, $\Gamma(u,c)$ is simply set to the sum of the SNRs corresponding to all TSs
3: **end for**   in the candidate set c that have been known from the SISO feedback of the STA u.
4: **repeat**
5:     $\mathbf{c}_{\text{Setup}} \leftarrow$ TransmitAntConfigForSetup(Γ);   // Step 1: Once the lookup table Γ is given, the collections $\mathbf{c}_{\text{Setup}}$
6:     $\mathbf{c}_{\text{Train}} \leftarrow$ TransmitAntConfigForTraining(Γ);   and $\mathbf{c}_{\text{Train}}$, and the set c_{poll}^u are obtained in the same
7:     **for each** STA $u \in \mathbf{u}_{\text{Tot}}$ **do**   manner identical to that described in Section III-C.
8:         $c_{\text{poll}}^u \leftarrow$ TransmitAntConfigForPolling(Γ, u);
9:     **end for**
10:    $\Gamma \leftarrow$ UpdateLookupTable($\Gamma, \mathbf{c}_{\text{Setup}}$);   // Step 2: Considering the determined transmit antenna configurations $\mathbf{c}_{\text{Setup}}$,
11:    $\Gamma \leftarrow$ UpdateLookupTable($\Gamma, \mathbf{c}_{\text{Tain}}$); $\mathbf{c}_{\text{Train}}$, and c_{poll}^u, our DTAC scheme checks if the lookup table Γ
12:    **for each** STA $u \in \mathbf{u}_{\text{Tot}}$ **do**   needs to be updated; to this end, Algorithm 2 is used.
13:        $\Gamma \leftarrow$ UpdateLookupTable($\Gamma, \{c_{\text{poll}}^u\}$);
14:    **end for**
15: **until** there are no updates in Γ // Step 3: Repeat Steps 1 and 2 until Γ has not been changed.

Algorithm 2 Function to update the lookup table, Γ

1: **function** UpdateLookupTable($\Gamma_{in}, \mathbf{c}_{\text{in}}$)
2:     **for each** STA $u \in \mathbf{u}_{\text{Tot}}$ **and each** candidate set $c = \{\alpha_1, \cdots, \alpha_{N_t}\} \in \mathbf{c}_{\text{in}}$ **do**
3:         **if** $\Gamma_{in}(u,c)$ has never been updated **and** $r_\alpha^u < \delta_{mu} + r_\delta \ for \ \forall \alpha \in c$ **then**
4:             $\Gamma_{in}(u,c) \leftarrow$ DNNBasedSNREstimation(R_{fb}^u, R_c^u);
5:         **end if**
6:     **end for**   // If the SNRs corresponding to the TSs in the set c, which are known from the SISO
7:     **return** Γ_{in} feedback of STA u, are all less than the SNR threshold δ_{mu} plus a predetermined margin value r_δ,
8: **end function**   our proposed scheme updates $\Gamma_{in}(u,c)$ to SNR estimated from the DNN
9:   in the manner identical to that described in Section III-B.
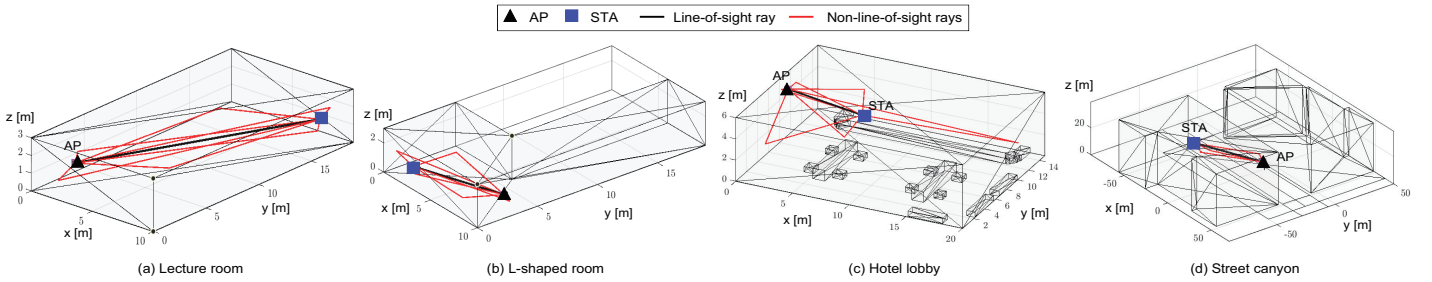

Fig. 5. Visualization of our evaluation scenarios: (a) Lecture room, (b) L-shaped room, (c) hotel lobby, and (d) street canyon.
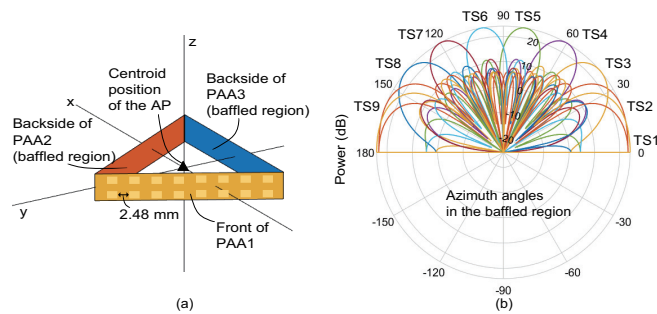

Fig. 6. (a) Visualization of three PAAs of the AP, i.e., PAAs 1 to 3, and (b) azimuth-cut patterns of nine TSs which are associated with each PAA.

primary simulation modules are as follows:

Q-D channel model with four scenarios: To accurately predict the characteristics of the mmWave channel, we employed the NIST Q-D channel realization software. We considered one AP and 11 STAs, and the channel between the AP and each STA was characterized by the direct and first-order reflected multipath components. In addition, pathloss, delay, phase shift, angle of arrival, and angle of departure were calculated as the properties of the respective multipath components. In our evaluation scenarios, the AP had three PAAs, and each STA used one PAA to realize a quasi-omni-receive pattern. In contrast to [7], the direct and specular multipath components were independently generated for each PAA of the AP. This is because the channel was weakly correlated when the centroid positions of the PAAs were mutually separated by a distance greater than one half-wavelength [32].

The indoor and outdoor scenarios of the lecture room, L-shaped room, hotel lobby, and street canyon were considered, as shown in Fig. 5, the AP was always fixed at a position, and the STAs were randomly located. To be precise, the AP was fixed at the coordinates $(1,3,1)$, $(9,3,1)$, $(1,7.5,5.5)$,

and $(0.78, -10, 6)$ m for the lecture room, L-shaped room, hotel lobby, and street canyon, respectively. We conducted simulations using two different modes, as described below.

1) *Purely-deterministic (PD) mode*: In this mode, the Q-D channel realization software captured only deterministic rays, i.e., line-of-sight and first-order reflected rays, obtained using ray tracing. The reflection loss of every specular ray was a constant value that had been predefined according to the material of the reflecting surface.

2) *Stochastic diffuse scattering mode*: In addition to the strong deterministic rays, we considered weaker rays which were generated due to the scattering of the specular rays from rough surfaces; we defined a *cluster* as a set of a deterministic ray and the corresponding diffuse rays. The properties of the diffuse rays and their reflection loss were obtained stochastically based on a measurement campaign conducted by NIST [18] in the scenarios of lecture room and L-shaped room; however, in the scenarios of hotel lobby and street canyon, these properties were stochastically obtained using measurements given in the TGay channel document [19].

Antenna model: We utilized three uniform planar arrays to represent the PAAs of the AP; each array had sixteen elements, i.e., 2×8, the elements were spaced at a distance of one half-wavelength from each other. As shown in Fig. 6, PAAs 1 to 3 were rotated with respect to the z-axis by $-30°$, $210°$, and $90°$, respectively, from the yz-plane. The total number of TSs were 27, and Fig. 6(b) shows the azimuth-cut patterns of the nine TSs associated with each PAA. The azimuth angles outside the interval $[0, 180]$ were located in the baffled region because we assumed that the radiation pattern was obstructed by the printed circuit board of each PAA. The codebook generator in [32] generated a steering vector representing the relative phases at a PAA, and the steering vector was used to calculate the AWVs of the TSs.

Link-level simulation: Using the properties of multipath components and the steering vector of the PAAs, the link-level simulator calculated the channel impulse response of the beamformed channel. In contrast to [7], it additionally considered stochastic diffuse multipath components and reflection loss in a manner identical to that in [25] and [31].

Let C and M be the total number of the clusters and the number of all deterministic and diffuse rays in the clusters, respectively. Then, referring to (29) in [7], the channel impulse response of the beamformed channel between the sth PAA and a receive PAA is as follows:

$$
\begin{aligned}
&h_s^{BF}(t) \\
&= \frac{1}{\sqrt{C}} \sum_{m=1}^{M} \Bigg(10^{PG_m/20} \cdot e^{j(-2\pi f t_m + \Psi_m)} \\
&\quad \times \delta(t - t_m) \cdot \mathbf{w}_r \times \mathbf{a}_r(\phi_m^a, \theta_m^a) \times \mathbf{a}_t(\phi_m^d, \theta_m^d)^* \cdot \mathbf{w}_t \Bigg),
\end{aligned}
$$
(3)

where $\mathbf{w}_t$, $\mathbf{w}_r$, and f are the weight vectors of transmit and receive PAAs and the operating frequency of the system, respectively; ϕ_m^a (θ_m^a) and ϕ_m^d (θ_m^d) are the azimuth (elevation) angles of arrival and departure; t_m is the arrival delay for the

m^{th} ray; $\delta(\cdot)$ is the Dirac delta function; $\mathbf{a}_t(\cdot)$ and $\mathbf{a}_r(\cdot)$ are the steering vectors of the transmit and receive PAAs; Ψ_m is the phase shift; PG_m is the path gain and it is obtained from (3) and (4) in [25] considering the reflection loss.

Referring to [38], the channel impulse response, $h_s^{BF}(t)$ in (3), is used to calculate the channel vector which employs an equivalent uniformly spaced tapped delay line. Let $h_{s,p}$ be the channel vector and the channel coefficient for the delay of the pth tap in units of single carrier chip time, denoted by T_c, between the sth transmit and receive antenna arrays. Then, considering a data block of L symbols, the channel vector for the sth transmit antenna array is given by

$$
\mathbf{h}_s = [h_{s,1},\ h_{s,2},\ \cdots,\ h_{s,p},\ \cdots,\ h_{s,\nu}, \cdots, 0], \quad (4)
$$

where the number of elements in the channel vector is L, i.e., $|\mathbf{h}_s| = L$, and ν is the number of delay taps of the channel.

Let $\mathbf{h}_{cir}$ be the channel vector obtained when all antenna arrays have been used with the cyclic shift diversity. Then, using (4), $\mathbf{h}_{cir}$ is given by

$$
\mathbf{h}_{cir} = \sum_{s=1}^{N_t} S(\mathbf{h}_s, \delta_s), \quad (5)
$$

where δ_s is a time shift for the cyclic shift diversity [3] and $S(\cdot)$ cyclically shifts the vector $\mathbf{h}_s$ to the right by δ_s / T_c.

To simply calculate the average signal to interference plus noise ratio (SINR), we use an $L \times L$ Toeplitz matrix, denoted by $\mathbf{H}_{toe}$, whose first row is $\mathbf{h}_{cir}$ in (5). We assume that the minimum mean-square error equalizer is applied to calculate the SINR; then, referring to [39] and [7], the average SINR measured at STA u for the transmission corresponding to a set $c \in \mathbf{c}_{Tot}$, is given by

$$
\gamma_{toe}^{MMSE}(u, c) = \left[\frac{1}{L} \times \sum_{k=1}^{L} \frac{1}{1 + \varphi \cdot (\|\lambda_k\|_2)^2} \right]^{-1} - 1, \quad (6)
$$

where $\{\lambda_k\}_{k=1}^{L}$ are the eigenvalues of $\mathbf{H}_{toe}$ and given $\mathbf{h}_{cir} = [h_1^{cir}, \cdots, h_\nu^{cir}, 0, \cdots, 0]$, it is computed as $\lambda_k = \sum_{l=1}^{\nu} h_l^{cir} e^{-j \frac{2\pi(l-1)(k-1)}{L}}$.

According to the algorithm of LSB, LNS, ILQE, or the proposed scheme, the transmit antenna configuration, i.e., sets of TSs, was determined. The link-level simulator then measured the packet error rate of each action frame transmitted through the selected set of TSs. Accordingly, we utilized the encoding and modulation schemes of the control mode implemented in the MATLAB WLAN toolbox and applied additive white Gaussian noise.

DNN model: We set the number of hidden layers to 3 [34]; the first, second, and third hidden layers comprised 128, 64, and 32 neurons, respectively, and the rectified linear unit (ReLU) activation function was used. We adopted mini-batches of size 32 and chose mean squared error (MSE) as the loss function. The adaptive moment estimation (Adam) optimizer was employed with a learning rate of 0.001 [40]. For each scenario, a dataset of 801,900 samples was collected and 90% and 10% of the samples were used to train and validate our DNN, respectively. Furthermore, each sample included input (R_{fb}^u, R_c^u) and the corresponding output SNR.
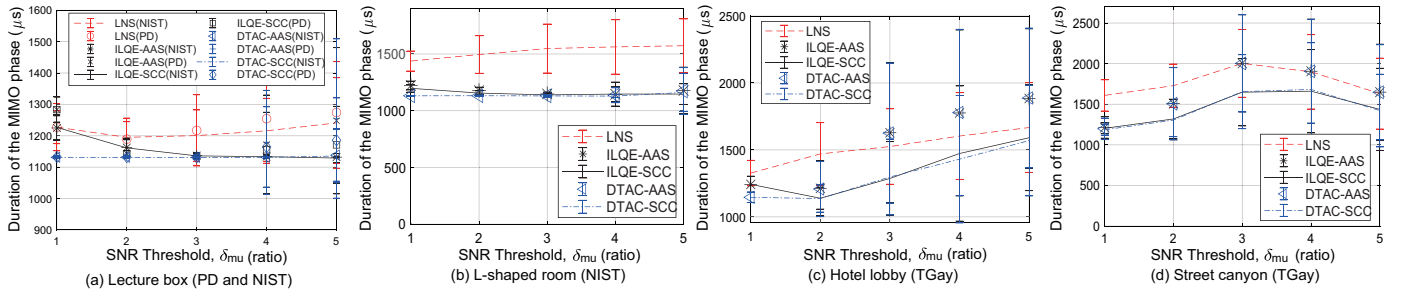
Fig. 7. Duration of the MIMO phase in the scenarios of (a) lecture room, (b) L-shaped room, (c) hotel lobby, and (d) street canyon.
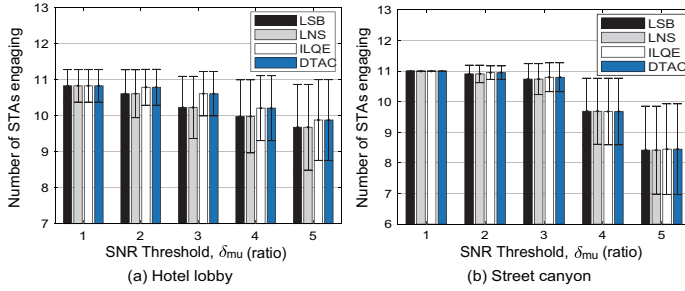

Fig. 8. Number of STAs engaging in the MIMO phase for the scenarios of (a) hotel lobby and (b) street canyon.

System-level simulation: Our ns-3 program conducted the MU-MIMO BFT at every beacon interval of approximately 0.1 s. Accordingly, we used the transmit antenna configurations and the corresponding packet error rates that had been obtained from the link-level simulation. The running time of a simulation trial was 100 s; hence, approximately 1,000 BFTs were conducted during the trial.

B. Delay and Signaling Overhead

We first evaluated the duration of the MIMO phase. To this end, we considered all cases in which the STAs failed to receive action frames transmitted by the AP, as described in [7]. In particular, we considered the case in which a STA was unable to transmit a BF feedback frame in the BF feedback subphase.

Figs.7(a)-(d) plot the duration of the MIMO phase in four different scenarios. In the simulations, all the STAs were allowed to engage in the MIMO phase for the scenarios of lecture room and L-shaped room; however, as shown in Figs. 8(a) and (b), certain STAs were not allowed to engage for the scenarios of hotel lobby and street canyon because they were expected to be outside the reach of the AP's transmission. The ILQE and DTAC schemes allowed more STAs to engage. Hence, those schemes considered two situations as follows [7]: First, the ILQE and DTAC schemes were performed under the same conditions as comparison schemes (SCC); i.e., those schemes performed the MIMO phase with STAs that the LSB and LNS schemes could support. Second, the ILQE and DTAC schemes conducted the BFT with all available subgroups (AAS) of the STAs in the MU group that could be reached by the AP's transmission.

It was observed that, in all scenarios, the durations of the ILQE and our DTAC schemes were shorter than those of the LSB and LNS schemes for the same conditions, i.e., in the SCC situation. The duration of LSB was considerably longer than that of the other schemes, and that is why the figures do not include the results of LSB. The curves in the figures can be attributed to the fact that the ILQE and DTAC schemes were able to transmit fewer action frames than the LSB and LNS schemes by identifying more STAs within reach of each transmission.

In particular, Table II presents the performance of each scheme for a threshold $\delta_{mu} = 3$ in the respective subphases of the MIMO phase. We found that in all subphases, the performance of the LSB scheme was significantly worse than that of the other schemes. The ILQE and DTAC schemes outperformed the LNS scheme, especially in the BF setup, training, and selection subphases for the same conditions.

The duration of the BF feedback subphase was determined using the following three factors: 1) the number of STAs engaging in the MIMO phase, 2) the probability of an STA not being able to transmit the BF feedback frame, and 3) the probability of an STA being unable to receive the BF poll frame. Figs.9(a)–(d) plot the second factor in the above-mentioned simulation scenarios. As described in [7], an STA cannot transmit the BF feedback frame if it fails to receive any BF setup or BRP-RX/TX frames. We observed that, in most cases, our proposed DTAC scheme had lower failure probabilities than the other schemes, which means that our proposed scheme enabled the STAs to receive the BF setup and BRP-RX/TX frames with higher link qualities.

C. Accuracy and Complexity of DNN-based Estimation

In our proposed DTAC scheme, the AP estimates each SNR measured at each STA when it transmits multiple concurrent beams. Considering the SNRs estimated, the AP identifies which STAs are within the reach of the multibeam concurrent transmission.

Our DTAC scheme employs DNN in a manner identical to that described in Section III-B. Fig. 10 illustrates the MSEs of our DNN-based estimation. To estimate the SNR measured at a STA when multiple concurrent beams are transmitted. Our DNN utilized the two sets of SNRs for its input: the first set was a set of all SNRs that were included in the SISO feedback of the STA, and the second set was a set of SNRs in the SISO feedback corresponding to the respective beams of the multiple

TABLE II
PERFORMANCE OF EACH SUBPHASE IN THE MIMO PHASE BY SETTING THE SNR THRESHOLD TO 3 ($\delta_{mu} = 3$).

| Scenario	Scheme	Duration of each subphase in MIMO phase (μs)				Duration of MIMO phase (μs)	# of action frames used in BF setup subphase	# of action frames used in BF training subphase
		BF setup	BF training	BF feedback	BF selection			
Lecture box (NIST)	LSB	76.72	798.84	865.61	268.33	2036.51	2.83	4.56
	LNS	26.58	181.63	867.7	97.67	1200.59	1.05	1.05
	ILQE-SCC	25.17	172.84	818.1	92.88	1135.99	1	1
	DTAC-SCC	25.17	172.84	813.28	92.88	1131.17	1	1
L-shaped room (NIST)	LSB	79.82	855.11	1073.22	278.88	2314.04	2.94	4.88
	LNS	37.57	271.31	1077.4	135.06	1548.12	1.44	1.56
	ILQE-SCC	25.17	172.84	821.54	92.88	1139.44	1	1
	DTAC-SCC	25.17	172.84	812.58	92.88	1130.47	1	1
Hotel lobby (TGay)	LSB	95.31	1486.38	900.88	328.72	2838.19	3.49	8.47
	LNS	46.58	385.61	901.91	164.3	1525.4	1.76	2.21
	ILQE-SCC	38.69	324.06	759.47	137.58	1286.82	1.48	1.86
	DTAC-SCC	38.97	334.61	758.8	138.54	1297.94	1.49	1.92
Street canyon (TGay)	LSB	84.04	1373.84	1101.62	293.26	2868.29	3.09	7.83
	LNS	55.87	630.03	1103.05	197.38	2002.97	2.09	3.6
	ILQE-SCC	50.52	593.1	798.85	179.16	1648.65	1.9	3.39
	DTAC-SCC	49.96	603.65	797.49	177.25	1655.36	1.88	3.45
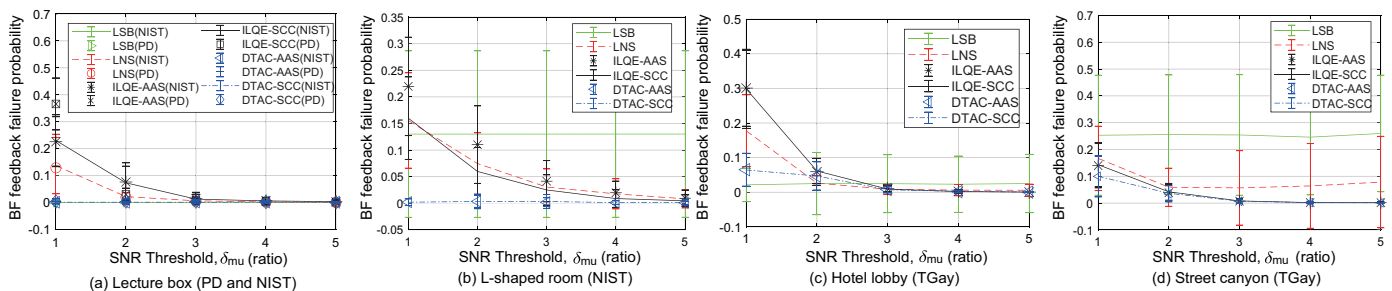
Fig. 9. Probability of an STA being unable to transmit the BF feedback frame for the scenarios of (a) lecture room, (b) L-shaped room, (c) hotel lobby, and (d) street canyon.
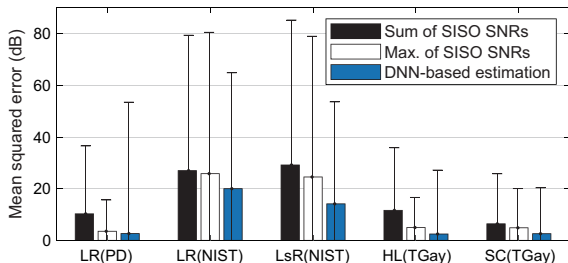

Fig. 10. MSEs of our DNN-based method in comparison with two SISO-based methods for the scenarios of lecture box (LB), L-shaped room (LsR), hotel lobby (HL), and street canyon (sc).

concurrent beams. We trained the DNN in a manner identical to that mentioned earlier in this section.

Fig. 10 demonstrates that our DNN-based estimation had lower MSEs in comparison to two other SISO-based methods; in the first SISO-based method, the SNR of the multiple concurrent beams was estimated to be the sum of SNRs corresponding to all its single beams. In the second method, the SNR was estimated to be the maximum value of the SNRs corresponding to all the single beams. We found that the MSEs in the scenarios of lecture room and L-shaped room were larger than those in the other scenarios. This is because, in the scenarios of lecture room and L-shaped room, the simulations were conducted in the stochastic diffuse scattering mode with NIST measurements. In this NIST mode, the angular spread of

diffuse rays in both elevation and azimuth planes followed a Laplacian distribution with zero mean and variance ρ^2 where ρ was randomly determined from Rician distribution [32].

Our DTAC and ILQE schemes required additional time to estimate SNRs measured at the STAs when the candidate sets of TSs (i.e., multiple beams) were used, in comparison to the LSB and LNS schemes. Figs. 11(a)–(d) plot the average number of estimations that our proposed DTAC and ILQE schemes conducted to determine an appropriate set of TSs to be used for the transmission of an action frame. We observed that, on average, the number of estimations required by our DTAC scheme was 96% less than that of the ILQE scheme without a heuristic method. This is because in the absence of the heuristic method, the ILQE scheme had to perform the estimation for all combinations of TSs that were included in at least one of the SISO feedback received from the STAs.

For each estimation, our proposed scheme performed a *forward pass*; i.e., the input SNRs was propagated forward through the DNN to compute the output SNR. In our simulations, because we used a simple multilayer perceptron with three hidden layers, the time complexity for the forward pass process was $O(n_i n_{h1} + n_{h1} n_{h2} + n_{h2} n_{h3})$, where n_i is the number of neurons in the input layer, and n_{h1}, n_{h2}, and n_{h3} are the number of neurons in the hidden layer1, 2, and 3, respectively. However, the time complexity of the estimation can be reduced when a lookup table is employed. This lookup
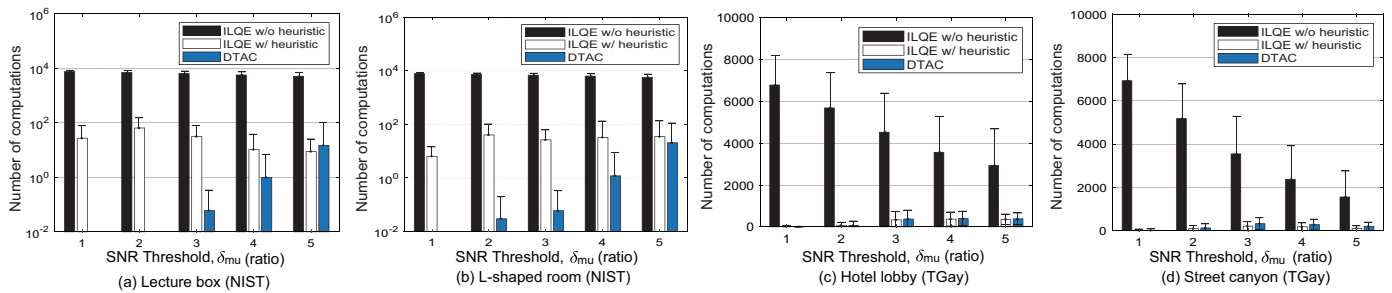
Fig. 11. Number of times the SNRs are estimated in ILQE without a heuristic method, ILQE with a heuristic method, and our DTAC scheme.

table contains the outputs precomputed using the DNN over discrete inputs [41].

V. CONCLUSION

The MU-MIMO data transmission of IEEE 802.11ay must be directional. To achieve this, an AP performs MU-MIMO BFT with STAs in the MU group. The signaling and latency overheads of MU-MIMO BFT primarily depend on how the AP selects TSs to transmit action frames. However, if the AP is incapable of efficiently estimating the SNRs to be measured at the STAs when certain TSs are used, it cannot select the appropriate TSs to transmit action frames during the MU-MIMO BFT. In this study, we propose a DTAC scheme that accurately estimates SNRs using a pretrained DNN. In contrast to the existing ILQE scheme, our proposed scheme refrains from collecting any additional information of the channel between the AP and STAs for the transmission of action frames. We also developed a heuristic method to reduce the computational complexity of the SNR estimation. We conducted extensive simulations, and the results revealed that our DTAC outperformed the existing schemes in terms of signaling and latency overhead. The simulation results also demonstrate that our heuristic method significantly reduces the number of times SNRs is estimated by the pretrained DNN.

REFERENCES

[1] S. Huang, M. Xiao, and H. V. Poor, "Achievable rate analysis of millimeter wave channels using random coding error exponents," *IEEE Trans. Wireless Commun.*, vol. 21, no. 1, pp. 250–263, Jan. 2022.

[2] S. Blandino *et al.*, "Markov multi-beamtracking on 60 GHz mobile channel measurements," *IEEE Open J. Veh. Technol.*, Early Access.

[3] *Enhanced Throughput for Operations in License-exempt Bands above 45 GHz*, IEEE Standard 802.11ay-2021, Jul. 2021.

[4] Y. Ghasempour, C. R. C. M. da Silva, C. Cordeiro, and E. W. Knightly, "IEEE 802.11ay: Next-generation 60 GHz communication for 100 Gb/s Wi-Fi," *IEEE Commun. Mag.*, vol. 55, no. 12, pp. 186–192, Dec. 2017.

[5] P. Zhou *et al.*, "IEEE 802.11ay based mmWave WLANs: Design challenges and solutions," *IEEE Commun. Surv. Tutor.*, vol. 20, no. 3, pp. 1654–1681, Mar. 2018.

[6] M-S. Kim, T. Ropitault, S.K. Lee, and N. Golmie, "Efficient MU-MIMO beamforming protocol for IEEE 802.11ay WLANs," *IEEE Commun. Lett.*, vol. 23, no. 1, pp. 144–147, Jan. 2019.

[7] M-S. Kim *et al.*, "A link quality estimation-based beamforming training protocol for IEEE 802.11ay MU-MIMO communications," *IEEE Trans. Commun.*, vol. 69, no. 1, pp. 634–648, Jan. 2021.

[8] Y. Ghasempour, M. K. Haider, and E. W. Knightly, "Multi-user multi-stream mmWave WLANs with efficient path discovery and beam steering," *IEEE J. Sel. Areas Commun.*, vol. 37, no. 2, pp. 2744–2758, Dec. 2019.

[9] Y. Ghasempour, M. K. Haider, and E. W. Knightly, "Decoupling beam steering and user selection for MU-MIMO 60-GHz WLANs," *IEEE-ACM Trans. Netw.*, vol. 26, no. 5, pp. 2390–2403, Oct. 2018.

[10] S. Blandino *et al.*, "Multi-User Hybrid MIMO at 60 GHz Using 16-Antenna Transmitters," *IEEE Trans. Circuits Syst. I*, vol. 66, no. 2, pp. 848–858, Feb. 2019.

[11] W. Wu *et al.*, "Fast mmWave beam alignment via correlated bandit learning," *IEEE Trans. Wireless Commun.*, vol. 18, no. 12, pp. 5894–5908, Dec. 2019.

[12] N. J. Myers, A. Mezghani, and R. W. Heath, Jr., "FALP: Fast beam alignment in mmWave systems with low-resolution phase shifters," *IEEE Trans. Commun.*, vol. 67, no. 12, pp. 8739–8753, Dec. 2019.

[13] C. Chen, O. Kedem, C. R. C. M. da Silva and C. Cordeiro, "Millimeter-wave fixed wireless access using IEEE 802.11ay," *IEEE Commun. Mag.*, vol. 57, no. 12, pp. 98–104, Dec. 2018.

[14] K. Aldubaikhy, W. Wu, N. Zhang, N. Cheng, and X. Shen, "MmWave IEEE 802.11ay for 5G fixed wireless access," *IEEE Wireless Commun.*, vol. 27, no. 2, pp. 88–95, Apr. 2020.

[15] L. H. Shen, K. T. Feng, and L. Hanzo, "Coordinated multiple access point multiuser beamforming training protocol for millimeter wave WLANs," *IEEE Trans. Veh. Technol.*, vol. 69, no. 11, pp. 13875–13889, 2020.

[16] Y. Kim, S. Lee, and T. Ropitault, "STS adaptation for beamforming training of asymmetric links in IEEE 802.11ay-based dense networks," in *Proc. IEEE VTC-Spring* 2020.

[17] A. Bodi, J. Zhang, J. Wang, and C. Gentile, "Physical-layer analysis of IEEE 802.11ay based on a fading channel model from mobile measurements," *in Proc. IEEE ICC*, 2019.

[18] C. Lai *et al.*, "Methodology for multipath-component tracking in millimeter-wave channel modeling," *IEEE Trans. Antennas Propag.*, vol.67, no.3, pp. 1826–1836, Mar. 2019.

[19] A. Maltsev et al., "Channel models for IEEE 802.11ay," IEEE Standard 802.11-15/1150r0, 2017.

[20] N. Varshney *et al.*, "Quasi-deterministic channel propagation model for an urban environment at 28 GHz," *IEEE Antennas Wiresless Propag. Lett.*, vol. 20, no. 7, pp. 1145–1149, 2021.

[21] C. da Silva, J. Kosloff, C. Chen, A. Lomayev, and C. Cordeiro, "Beamforming training for IEEE 802.11ay millimeter wave systems," in *Proc. ITA*, 2018.

[22] H. Echigo, Y. Cao, M. Bouazizi, and T. Ohtsuki, "A deep learning-based low overhead beam selection in mmWave communications," *IEEE Trans. Veh. Technol.*, vol. 70, no. 1, pp. 682–691, Jan. 2021.

[23] L.-H. Shen, T.-W. Chang, K.-T. Feng, and P.-T. Huang, "Design and implementation for deep learning based adjustable beamforming training for millimeter wave communication systems," *IEEE Trans. Veh. Technol.*, vol. 70, no. 3, pp. 2413–2427, Mar. 2021.

[24] P. Zhou, *et al.*, "Deep learning-based beam management and interference coordination in dense mmWave networks," *IEEE Trans. Veh. Technol.*, vol. 68, no. 1, pp. 592–603, Jan. 2019.

[25] M. Lecci et al., "Quasi-deterministic channel model for mmWaves: Mathematical formalization and validation," in *Proc. IEEE Globecom*, 2020.

[26] T. Bai and R. W. Heath, Jr., "Coverage and rate analysis for millimeterwave cellular networks," *IEEE Trans. Wireless Commun.*, vol. 14, no. 2, pp. 1100–1114, Feb. 2015.

[27] J. G. Andrews, *et al.*, "Modeling and analyzing millimeter wave cellular systems," *IEEE Trans. Commun.*, vol. 65, no. 1, pp. 403–430, Jan. 2017.

[28] M. Baianifar, S. M. Razavizadeh, H. Akhlaghpasand and I. Lee, "Energy efficiency maximization in mmWave wireless networks with 3D beamforming," *J. Commun. Netw.*, vol. 21, no. 2, pp. 125–135, Apr. 2019.

[29] M. R. Akdeniz et al., "Millimeter wave channel modeling and cellular capacity evaluation," *IEEE J. Sel. Areas Commun.*, vol. 32, no. 6, pp. 1164–1179, Jun. 2014.

[30] *Study on channel model for frequencies From 0.5 to 100 GHz, document (TR) 38.901*, 3GPP, Jun. 2018.

[31] M. Lecci, P. Testolina, M. Polese, M. Giordani, and M. Zorzi, "Accuracy versus complexity for mmWave ray-tracing: A full stack perspective," *IEEE Trans. Wireless Commun.*, vol. 20, no. 12, pp. 7826–7841, Dec. 2021.

[32] H. Assasa and T. Ropitault, "A collection of open-source tools to simulate IEEE 802.11ad/ay WLAN networks in ns-3," 2019. [Online]. Available: https://github.com/wigig-tools

[33] N. Varshney, J. Zhang, J. Wang, A. Bodi, and N. Golmie, "Link-level abstraction of IEEE 802.11ay based on quasi-deterministic channel model from measurements," in *Proc. IEEE VTC2020-Fall*, 2020.

[34] J. Wang, N. Varshney, J. Zhang, D. Griffith, and N. Golmie. "Deep learning based link-level abstraction for mmWave communications," in *Proc. IEEE SmartWorld/SCALCOM/UIC/ATC/IOP/SCI*, 2021.

[35] H. Assasa, J. Widmer, T. Ropitault, and N. Golmie, "Enhancing the ns-3 IEEE 802.11ad model fidelity: Beam codebooks, multi-antenna beamforming training, and quasi-deterministic mmWave channel," *in Proc. Workshop Ns-3*, 2019.

[36] H. Assasa, *et al*., "Implementation and evaluation of aWLAN IEEE 802.11ay model in network simulator ns-3," *in Proc. Workshop Ns-3*, 2021.

[37] J.-S. Sheu, "Hybrid digital and analogue beamforming design for millimeter wave relaying systems," *J. Commun. Netw.*, vol. 19, no. 5, pp. 461–469, 2017.

[38] C. D. Iskanderp, "A matlab-based object-oriented approach to multipath fading channel simulation," *Hi-Tek Multisystems* vol 21, pp. 1–15, Feb. 2008.

[39] A.H. Mehana and A. Nosrantinia, "Single-carrier frequency-domain equalizer with multi-antenna transmit diversity," *IEEE Trans. Wireless Commun.*, vol. 12, no. 1, pp. 388–397, Jan. 2013.

[40] S. Moon, H. Kim and I. Hwang, "Deep learning-based channel estimation and tracking for millimeter-wave vehicular communications," *J. Commun. Netw.*, vol. 22, no. 3, pp. 177–184, Jun. 2020.

[41] Y. Sekikawa and T. Suzuki. "Tabulated MLP for fast point feature embedding," 2019. [Online]. Available: https://arxiv.org/abs/1912.00790

SuKyoung Lee (Member, IEEE) received the B.S., M.S., and Ph.D. degrees from Yonsei University, Seoul, South Korea, in 1992, 1995, and 2000, respectively, all in Computer Science. From 2000 to 2003, she was with the Advanced Networking Technologies Division, National Institute of Standards and Technology, Gaithersburg, MD, USA. She is currently a Professor with the Department of Computer Science, Yonsei University. Her current research interests include wireless networking, mobile/edge systems, and vehicular networks.

Jun-Hyeok Choi is currently working toward the B.S. degree in the Department of Computer Sciences and Engineering, Sejong University, Seoul, Korea. His research interests focus on AI and metaverse.

Mun-Suk Kim received the B.S., M.S., and Ph.D. degrees in Computer Science from Yonsei University, Seoul, South Korea, in 2007, 2009, and 2016, respectively. From 2016 to 2021, he worked as a Guest Researcher with the Communications Technology Laboratory, National institute of Standards and Technology, Gaithersburg, MD, USA. He is currently an Assistant Professor with the Department of Computer Sciences and Engineering, Sejong University. His research interests include mobility management, resource allocation, mathematical modeling, and the application of machine learning to problems in computer networking.

Nada Golmie (Senior Member, IEEE) received the Ph.D. degree in Computer Science from the University of Maryland at College Park, College Park, MD, USA. Since 1993, she has been a Research Engineer with the National Institute of Standards and Technology. She is currently the Chief of the Communications Technology Laboratory, Wireless Networks Division. Her research interests include media access control and protocols for wireless networks led to more than 100 technical articles presented at professional conferences, journals, and contributed to international standard organizations and industry led consortia. She is the author of Coexistence in Wireless Networks: Challenges and System-Level Solutions in the Unlicensed Bands, (Cambridge University Press, 2006). She also leads several projects related to the modeling and evaluation of future generation wireless systems and protocols. She serves as a Co-Chair of the 5G mmWave Channel Model Alliance and leads the NIST Future Generation Communication Research and Development Roadmap.

Tanguy Ropitault received the Ph.D. degree in Computer Science from the Institut Mines Telecom, Rennes, France in 2015. He is currently a Contractor working with the Wireless Network Division, National Institute of Standards and Technology, Gaithersburg, MD, USA. His current research interest includes mmWave system-level performance evaluation.